Miner Deposita (2010) 45:51–68
DOI 10.1007/s00126-009-0261-3

ARTICLE

Textural variation in the pyrite-rich ore deposits of the Røros district, Trondheim Region, Norway: implications for pyrite deformation mechanisms

Craig D. Barrie · Nigel J. Cook · Alan P. Boyle

Received: 9 September 2008 / Accepted: 31 August 2009 / Published online: 2 October 2009

Abstract The Røros district is a pyrite-rich polymetallic sulfide orefield in the southeastern part of the Trondheim region, Central Norwegian Caledonides. All of the ore deposits at Røros are hosted within a Cambrian to Silurian succession that was deformed and metamorphosed at lower greenschist to lower amphibolite facies conditions during the Caledonian orogeny. Samples from five individual deposits across the orefield have been analyzed using a combination of reflected light petrographic observation, orientation contrast imaging, and electron backscatter diffraction. Results indicate that, whereas samples from each ore deposit have a variety of different textures, all of them preserve plastic deformation in pyrite grains that occurred at peak metamorphic conditions characterized by the development of internal lattice misorientation within pyrite grains and low-angle (~2°) dislocation walls. These observations indicate that the principal deformation mechanisms at peak metamorphic conditions were dislocation glide and creep. The preservation of brittle fracturing represents later overprinting events.

Keywords Røros · Pyrite · Norwegian Caledonides · EBSD · Dislocation creep

Editorial handling: H. Frimmel

C. D. Barrie · A. P. Boyle
Department of Earth and Ocean Sciences,
University of Liverpool,
Liverpool L69 3GP, England

N. J. Cook
School of Earth and Environmental Sciences,
University of Adelaide,
Adelaide, SA 5005, Australia

Present Address:
C. D. Barrie (✉)
School of Geography and Geosciences,
University of St. Andrews,
St. Andrews, Fife KY16 9AL, Scotland
e-mail: cdb21@st-andrews.ac.uk

Introduction

Pyrite is the most abundant sulfide mineral in the Earth's crust occurring in a diverse number of environments as well as predominantly in sulfide ore deposits (Mann et al. 1990; Craig and Vokes 1993; Craig et al. 1998). Many sulfide ore deposits have experienced deformation and/or metamorphism at some point after their formation, and understanding these effects on the textures and geochemistry of ore minerals is important for their successful exploitation (Vokes 1969; Marshall and Gilligan 1987; Castroviejo 1990; Gaspar and Pinto 1991; Brown and McClay 1993; Xu 1996; Allen et al. 2002; Freitag et al. 2004). The refractory nature of pyrite means it has the potential to record significant aspects of an ore deposit's metamorphic and deformation history (Craig and Vokes 1993).

Early studies of pyrite deformation suggested it behaved in a brittle manner at most levels and conditions in the Earth's crust (Gill 1969; Graf and Skinner 1970; Atkinson 1975), but subsequent work showed that it can deform plastically at temperatures as low as ~425˚C (Cox et al. 1981; Graf et al. 1981; McClay and Ellis 1983; Siemes et al. 1993). The most recent studies suggest that plastic deformation of pyrite is widespread and may occur at temperatures as low as ~325°C (Boyle et al. 1998; Freitag et al. 2004; Barrie et al. 2007). These last three studies demonstrate that plastic deformation of pyrite can be readily observed and quantified using electron backscatter diffraction (EBSD) techniques.

Ore deposits of the Røros district, Central Norwegian Caledonides, are well characterized with respect to their geological setting, but understanding of deformation and metamorphism of the sulfide ore minerals is limited. Rui and Bakke (1975) suggested that pyrite behaved in a brittle manner compared with the surrounding sulfides but expanded little on this observation. We seek to build upon the understanding of pyrite behavior by characterizing deformation textures and microstructures developed at the grain and subgrain scale in a series of pyrite-rich ore deposits from the Røros district, a classic volcanogenic massive sulfide (VMS) province (Vokes 1976) in which a number of texturally-distinct ores are found. This study aims to answer three main questions:

1. What primary and/or deformation textures are preserved within the sulfide minerals and specifically, pyrite grains, in the Røros ore deposits?
2. Which deformation mechanisms have operated at peak metamorphic conditions, and do these correspond with the textures preserved?
3. Is it possible to reconstruct the deformation and metamorphic history of the ore deposits based upon pyrite textures?

Tectonostratigraphic setting of the Røros ore deposits

The Scandinavian Caledonides are part of a belt of late Precambrian to early Paleozoic rocks emplaced as a series of thrust nappes during the Caledonian Orogeny (Roberts and Gee 1985; Hacker and Gans 2005). The belt constitutes the northernmost sector of the composite Caledonian–Appalachian belt, which stretches from northern Norway to Alabama (Grenne et al. 1999). Conditions of metamorphism vary from lower greenschist to upper amphibolite facies, and several phases of deformation have been recorded (Bryhni and Andreasson 1985) which are also reflected in the contained ore deposits (Craig and Vokes 1992). The nappes forming the Caledonides can be grouped into four main allochthons, the Lower, Middle, Upper, and Uppermost Allochthons (Roberts and Gee 1985).

The Røros district is located in the southeastern Trondheim region of Norway (approximately 62°35′N, 11°23′E), not far from the Swedish border (Fig. 1a; Rui and Bakke 1975) and is part of the Upper Allochthon, which comprises the Seve and overlying Köli Nappe systems. The Upper Allochthon consists of continental rocks thought to represent the outermost margin of Baltica plus ophiolitic rocks interpreted to represent chiefly Iapetus Ocean lithosphere (Hacker and Gans 2005). The district has experienced lower greenschist to lower amphibolite facies conditions during Scandian orogenesis (Grenne et al. 1999) and is host to a number of sulfide ore deposits (Fig. 1b) associated with Late Ordovician calcareous phyllites, metagraywackes, and local interlayers of possible volcanoclastic origin, which form part of a large, complexly folded synformal structure (Wolff 1967; Rui 1972; Rui and Bakke 1975; Grenne et al. 1999). The area has also been extensively intruded by a variety of gabbro and trondhjemite sills (Bjerkgård et al. 1999; Grenne et al. 1999), which assist to constrain age relationships in the region (Nilsen et al. 2003; Nilsen et al. 2007).

Regional tectonostratigraphy is complex, in parts poorly constrained, and the subject for debate. The Trondheim Nappe Complex, which, in turn is divided into the Gula, Støren, and Meråker Nappes, represents Köli rocks in the Southern Trondheim Region (Roberts and Wolff 1981; Gee and Sturt 1985). Köli sequences are recognized over a distance of more than 500 km north of Røros. The Røros district in the east of the Southern Trondheim region lies within the Meråker Nappe. This comprises the Fundsjø Group, essentially a basal mafic magmatic complex which underwent an Early Ordovician (pre-Scandian) tectonothermal event and a thick overlying turbidite sequence of Ordovician to Early Silurian age. The Fundsjø Group hosts the Killingdal deposit and ores of the Folldal orefield and is related to convergence rather than ocean closure (Vokes et al. 2003). Grenne et al. (1999) regarded the turbidites in the Meråker Nappe to represent oceanic sequences developed at a distance from the margin of Baltoscandia. In contrast, the Gula Nappe in the western part of the Southern Trondheim region is of probable continental margin or shelf origin. Some workers (Sturt et al. 1997; Sturt and Ramsay 2002) inferred a major unconformity within the Gula Nappe (McClellan 2004). It is clear, however, that, despite uncertainties over its early development, the entire Trondheim Nappe Complex underwent deformation and metamorphism at comparatively low metamorphic grades between lower greenschist and lower amphibolite facies during the Scandian Orogeny (Siluro-Devonian) with thrusting over the Seve nappes in the Middle Silurian in response to closure of the Iapatus (Ihlen et al. 1997).

Recent work (Sundblad et al. 2006) has placed all of the principal ore deposits in the Røros district within the Middle Köli turbidite sequence and proposes they may represent "Escanaba"-type VMS deposits implicitly formed nearer to the continental margin than previously believed. However, most of the Røros massive sulfide deposits (including Kongens Gruve, Nye Storwartz, and Klingenberg) occur in turbidite-dominant sequences (Røros Schists).

The ore deposits at Røros were continually exploited for over 300 years between 1644 and 1977 (Rui and Bakke 1975; Bjerkgård et al. 1999). Detailed descriptions and historical information can be found in the Geological Survey of Norway ore database (http://www.ngu.no). Renewed exploration in the past decade has indicated that

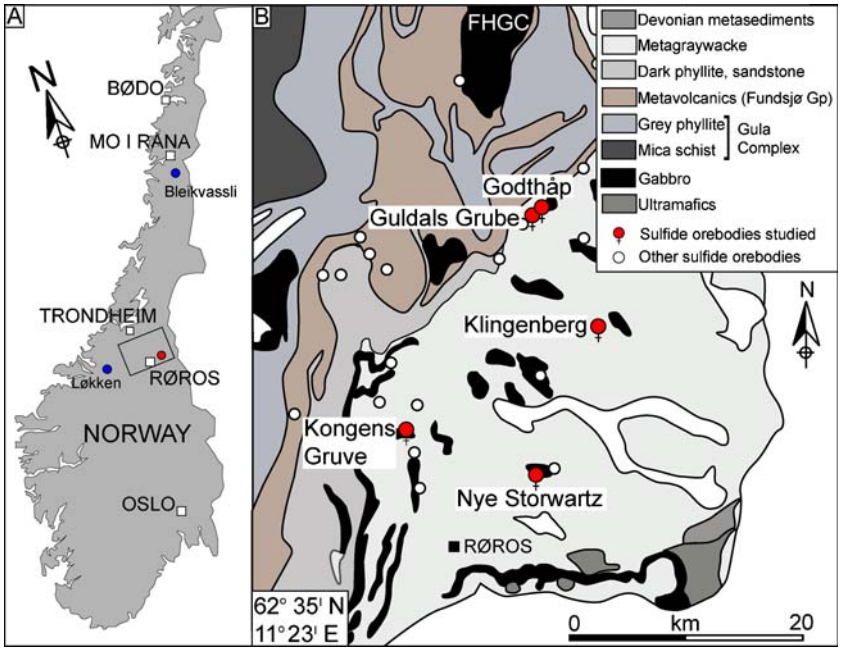

Fig. 1 **a** Map of Norway with the Røros district *highlighted*. **b** Geological map of the Røros district with locations of the main ore deposits in the area and those discussed in this study *highlighted*. *FHGC* Fongen-Hyllingen Gabbro Complex (modified after Grenne et al. 1999)

known deposits in the area contain significant in situ resources as well as potential future resources.

Sulfide mineralization consists of stratabound, mainly massive, ore deposits, which may be either pyrrhotite- or pyrite-dominant or contain both Fe sulfides (Rui and Bakke 1975; Bugge 1978). Total ore production from the mines in the Røros district was ~6.5 Mt. containing an average of c. 2.7% Cu and 4.2–5.0% Zn (Bjerkgård et al. 1999). Numerous smaller deposits occur throughout the area; most production came from the central part of the area north of Røros town (as well as from Killingdal). Alluding to their setting within thick turbidite sequences, some workers have chosen to describe the Røros ores as Besshi-type (Ihlen et al. 1997).

The massive sulfide ores are believed to have formed at the same time as Ni–Cu–Cr–(PGE) ores deeper in the crust in the area (Nilsson et al. 1997), or shortly thereafter. Orebody morphologies are tabular- or ribbon-shaped with long axes of lenses generally parallel to the regional fold axes and stretching lineations (Grenne 1987; Bjerkgård et al. 1999). Deposits are generally thought to be VMS in origin (Bjerkgård et al. 1999; Grenne et al. 1999). Although such a genesis is widely accepted, some workers have suggested a discordant nature between the sulfides and wall rock, potentially due to syndeformational remobilization and thrusting along the plane of the sulfide horizons superimposed on the possible primary volcano-exhalative stratabound character of the ores (Rui and Bakke 1975) based on the character of the host succession and comparison with volcano-exhalative ores elsewhere in the Caledonides.

Metamorphic conditions in the central portion of the Norwegian Caledonides preserve a general trend of increasing metamorphic grade from prehnite–pumpellyite facies at Løkken in the southwest (lat. 63°07′ long. 9°42′) to upper amphibolite facies at Bleikvassli in the northeast (Fig. 1a; lat. 65°50′ long. 13°50′) (Vokes 1976; Bryhni and Andreasson 1985; Skauli et al. 1992). The Røros district is suggested to preserve a similar trend with metamorphic grade of the ore deposits increasing in a northeasterly direction (Rui 1972). Whereas, it was not possible in this study to determine specific metamorphic conditions at each individual mine, the tectonic setting and associated host rock characteristics suggest these range between lower greenschist and lower amphibolite facies (Vokes 1988).

This study looks at samples of pyrite-rich ore from five mines across the Røros district (Fig. 1b; Table 1). Kongens Gruve, Klingenberg, and Nye Storwartz are larger massive sulfide deposits hosted within the Røros Formation in the central part of the district, whereas Godthåp and Guldals Grube are hosted within the Røsjo formation north of the main orefield (Bjerkgård et al. 1999). Both the Røros and Røsjo formations are Lower Ordovician in age. The Røsjo Formation underlies the Røros Formation with which it has a transitional boundary (Rui and Bakke 1975). If the interpretation of stratigraphic inversion is correct, this would make them slightly younger but still products of the main ore-forming event in the district.

Sampling and sample preparation

Several representative samples were examined from each location. Each specimen was prepared as 1-in. polished blocks suitable for reflected light microscopy and examined using a scanning electron microscope (SEM). Samples

Table 1 Summary table describing the main characteristics, textures, and fabrics present in the ore deposits investigated

Deposit	Location	Type	Mining history	Brief ore deposit description	Description of textures and fabrics
Kongens Gruve NGU: 1640.052	Røros Kommune	Cu–Zn	Underground mine 1657–1945, ca. 3 Mt ore exploited	Massive, semimassive, and banded ore; chalcopyrite, sphalerite, Gangue: pyrite, pyrrhotite, chlorite, quartz.	Fabrics: pyrite grain-size layering, weak chalcopyrite–sphalerite compositional layering. Fracture development is minimal. Pyrite grains generally appear equant.
Klingenberg NGU: 1640.061	Røros Kommune	Cu–Zn	Underground mine until 1907; exploration 1999–2001 on account of high Zn content	Massive ore; chalcopyrite, sphalerite, (galena). Gangue: pyrite, chlorite, quartz, (biotite, ampbibole).	Fabrics: pyrite grain-size layering, weak chalcopyrite-sphalerite compositional layering. Lensing of pyrrhotite. Extensive fracture development and occasional pyrite pulverization. Pyrite grains generally appear equant.
Nye Storwartz NGU: 1640.046	Røros Kommune	Cu–Zn	Underground mine until 1947; 150,000 t ore exploited; 75,000-t reserves	Massive ore; chalcopyrite, sphalerite. Gangue: pyrite, pyrrhotite, biotite, chlorite, ampbibole.	Fabrics: sphalerite–chalcopyrite compositional foliation or "lensing". Fracture development is, at best, minimal and generally absent. Pyrite grain boundaries have an irregular, embayed texture.
Guldals Grube NGU: 1644.028	Holtålen Kommune	Cu–(Zn)–(Pb)	Underground mine (pre-20th century)	Cu-rich ore; chalcopyrite, sphalerite, galena. Gangue: pyrite, pyrrhotite, biotite, hornblende, quartz. Semimassive; some evidence of brecciation.	Fabrics: shape preferred orientation of pyrite grains. Extensive fracture development and occasional pyrite pulverization. Development of ~120° triple-junctions at pyrite grain boundaries.
Godthåp NGU: 1644.025	Holtålen Kommune	Cu–(Zn)–(Pb)	Underground mine (pre-20th century)	Cu-rich ore; chalcopyrite, sphalerite, galena; gangue: pyrite, pyrrhotite, quartz.	Fabrics: shape preferred orientation of pyrite grains. Fracture development is minimal. Pyrite grain boundaries have an irregular, sutured texture.

studied using electron backscatter diffraction were further polished using a suspension of colloidal silica in sodium hydroxide solution (SYTON^{TM}) to remove physical damage caused by initial polishing. Not all polished blocks, however, could be sufficiently well polished due to inherent relief between coexisting minerals, the presence of abundant inclusions, and, in some specimens, rapid tarnishing immediately after polishing. Sample selection has therefore been biased by these requirements, but those selected for further study were characteristic of each ore deposit as well as the textures and mineral abundances as a whole.

The samples studied by EBSD and, implicitly, the choice of ore deposits covered using this method, therefore represent a subset of the total sample suite. The sample suite represents a first attempt to ascertain the variation in pyrite deformation mechanisms in ores across a larger region where all deposits share a common genetic history with respect to timing, broad geological setting, mineralogy, and postgenetic evolution yet differ significantly with respect to relative abundance of ore and gangue minerals, grain size, and superimposed effects of regional metamorphism.

Methodology

All pyrite crystallographic orientation data were collected at the University of Liverpool using a CamScan X500 crystal probe SEM with a thermionic field emission gun, accelerating voltage of 20 kV, and a typical beam current of ~5 nA. The angular resolution of this technique is typically better than 1° with a spatial resolution of ~0.05 μm (Ohfuji et al. 2005). EBSD data were processed using the software package CHANNEL+ v5 from Oxford Instruments. All of the samples contain significant proportions of other sulfides, predominantly sphalerite (ZnS) and chalcopyrite ($CuFeS_2$), but EBSD analysis of these phases was not possible due to polishing damage of these softer phases (Prior et al. 2002; Ohfuji et al. 2005; Barrie et al. 2007).

The processed pole figures are oriented with *XY* in the drawing plane, *Z* normal to the drawing plane, and *Y* vertical. All pole figures were plotted using the PFch5.exe program (Mainprice 1990). Misorientation angle distribution plots were also generated to determine relationships between correlated and uncorrelated grains within samples (Wheeler et al. 2001). A measure of crystallographic preferred orientation (CPO) was calculated using PFch5.exe to generate the pole figure J index (Michibayashi and Mainprice 2004).

Results

Results are presented starting with the most southwesterly deposit (Kongens Gruve) and finishing with the most

Table 2 Summary table of the mineral modes from a single polished section of each of the ore deposits investigated

Deposit	Pyrite	Sphalerite	Chalcopyrite	Galena	Pyrrhotite	Silicates
Kongens Gruve NGU: 1640.052	~70%	~15%	~15%	<1%	<1%	<1%
Nye Storwarts NGU: 1640.061	~60%	~10%	~25%	<1%	~5%	<1%
Klingenberg NGU: 1640.046	~50%	~25%	~25%	<1%	<1%	<1%
Guldals Grube NGU: 1644.028	~85%	~10%	~5%	–	–	<1%
Godthap NGU: 1644.025	~70%	–	~10%	<1%	~20%	<1%

northeasterly (Godthåp), thus reflecting the assumed increase in metamorphic grade.

Kongens Gruve (Røros Fm; Røros Kommune)

Kongens Gruve (Table 1; Fig. 1b) is characterized by relatively fine-grained pyrite-rich ore (Tables 2, 3; Fig. 2). There is a compositional foliation defined by sphalerite and chalcopyrite variation as well as an associated weak pyrite grain size layering (Fig. 3a). Sphalerite predominantly encloses large (~100 μm) pyrite grains while chalcopyrite encloses smaller (~40 μm) pyrite grains. Pyrite grains are predominantly idiomorphic, and pyrite–pyrite boundaries are generally long and curved (Fig. 3b). Inclusions are present within pyrite grains but not widespread and relatively small (<5 μm). Orientation Contrast (OC) Images (Fig. 4a) reveal internal gray-scale variation, and EBSD analysis shows that lattice rotation generally occurred about a single or two <100> axes with cumulative misorientation on average ~2° (Table 3; Fig. 5). Low-angle (~2°) subgrain boundaries are present within pyrite grains (Fig. 4b), but they are not widespread, and most are restricted to grain boundary regions. The neighbor-pair misorientation angle histogram is dominated by a low-angle (~2°) boundary peak twice that of the theoretical random peak at ~60° while random-pair misorientations are close to the theoretical random distribution for pyrite crystal orientations (Fig. 4c).

Nye Storwartz (Røros Fm; Røros Kommune)

Nye Storwartz, in the central region of the Røros district (Table 1; Fig. 1b), is characterized by relatively coarse grained, ~160 μm pyrite grains (Table 3; Fig. 2). There is a weak grain-size layering within the sample defined by ~300 μm and <100 μm pyrite domains. A weak compositional layering is also present between chalcopyrite and sphalerite while pyrrhotite tends to form discrete >5 mm lenses within the ore (Fig. 3c). Pyrite–pyrite grain boundaries tend to be curved and commonly have fracture zones emanating from the contact (Fig. 3d). Fracturing is preserved in most pyrite grains and many appear "pulverized" with fractures often filled by slivers of the surrounding minor phases (Fig. 3d). Most pyrite grains have inclusions of the surrounding sulfides, typically >10-μm in size (Fig. 3d). OC images (Fig. 6a, d) reveal internal gray-scale variation within pyrite grains indicative of lattice deformation. EBSD analysis shows lattice rotation occurred about a single or two separate <100> axes (Fig. 6a, d) with average cumulative misorientation of ~2° (Table 3; Fig. 5). Low-angle (~2°) subgrain boundaries can be found in most

Table 3 Summary table of the main textural characteristics found at each ore deposit. Foliations are defined as either compositional, grain size, or weak shape fabrics

Deposit	Grain size mean (μm)	Grain size range(μm)	EBSD mapped area	Lattice misorientation (mean)	Lattice misorientation (maximum)	Crystallographic preferred orientation (CPO)
Kongens Gruve NGU: 1640.052	~40	~200	~6 mm^2	~2°	~12°	No
Nye Storwartz NGU: 1640.061	~162	~310	~6 mm^2	~2°	~14°	No
Klingenberg NGU: 1640.046	~330	~700	~5 mm^2	~2°	~24°	No
Guldals Grube NGU: 1644.028	~280	~900	~5 mm^2	~2°	~8°	No
Godthap NGU: 1644.025	~30	~85	~8 mm^2	~4°	~36°	<111>

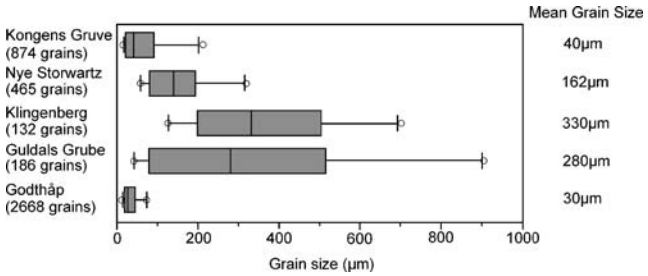

Fig. 2 *Box plots* summarizing grain size variation (all grains smaller than 10µm removed). Boxes represent the middle 50% of the data; the interquartile range. The *line* inside each box is the mean value of the data and the "*whiskers*" represent the extremes of the data (3/2 of the interquartile range). *Open circles* represent data regarded as outliers

pyrite grains, but they are not abundant; at most, only one or two are found within individual grains. The neighbor-pair misorientation angle histogram has a low-angle peak (~2°) double that of the theoretical random peak at ~60° while random pair misorientations are much closer to those expected for a theoretical random distribution of pyrite crystal orientations (Fig. 6e).

Klingenberg (Røros Fm; Røros Kommune)

Klingenberg is a coarse-grained pyrite-rich ore body in the central region of the Røros district (Tables 1, 2; Fig. 1b, 2). The sample studied has a weak compositional foliation or "lensing" defined by modal variation of chalcopyrite and sphalerite (Fig. 3e). Pyrite-grain shapes are irregular, and most grains are well rounded with large "embayments" filled by the surrounding phases (Fig. 3f). Pyrite–pyrite boundaries are straight or gently curved, but these contacts are rare in 2D section, and most pyrite is enclosed in a sphalerite/chalcopyrite matrix (Fig. 3e, f). Inclusions of the other sulfide phases up to ~50 µm in size are widespread in pyrite grains. Many of these inclusions and those filling embayed boundaries can be correlated with sulfide grains immediately outside the host pyrite making it possible to trace potential "ghost" phase boundaries through host pyrite grains.

OC images (Fig. 7) show obvious internal gray-scale variation, and EBSD analysis shows that lattice rotation occurred about either a single or two separate <100> axes. Cumulative misorientation in pyrite grains has a mean of ~2° (Table 3, Fig. 5). Low-angle (~2°) subgrain boundaries are present within pyrite grains (Fig. 7a) but are generally restricted to grain boundary regions and, more commonly, impingement zones (Fig. 7a). Misorientation profiles through pyrite grains suggest lattice rotation accumulates continuously in increments of ~1° or less (Fig. 7e). Neighbor-pair (correlated) misorientation angle histograms reveal a low-angle peak (~2°) twice that of the theoretical random peak at ~60° while random pair (uncorrelated) misorientations follow the theoretical random distribution of pyrite crystal orientations (Fig. 7f).

Guldals Grube (Røsjo Fm, Holtålen Kommune)

Guldals Grube is located in the northern part of the Røros district (Table 1; Fig. 1b) and is characterized by coarse-grained pyrite-rich ore (Table 3, Fig. 2). Pyrite grains are idiomorphic with generally long, straight boundaries between pyrite grains (Fig. 3g, h). Foam texture is indicated by common 120° triple junctions. Inclusions are not widespread in pyrite, but, where present, they are large (~50 µm) and consist primarily of chalcopyrite. Brittle fracturing is widespread and a few pyrite grains appear almost completely "pulverized". OC images (Fig. 8a) reveal internal gray-scale variation, and EBSD analysis shows lattice rotation occurred primarily about a single <100> axis (Fig. 8a) with just a few grains preserving lattice rotation of ~2–3° about a second <100> axis. Cumulative misorientation within pyrite grains is on average ~2° (Table 3, Fig. 5). Pyrite grains contain few low-angle (~2°) subgrain boundaries (Fig. 8b); misorientation profiles through grains indicate lattice misorientation accumulated continuously in increments of ~1° or less (Fig. 8c, d).

Godthåp (Røsjo Fm, Holtålen Kommune)

Godthåp is located in the northern part of the Røros district close to Guldals Grube (Table 1; Fig. 1b) and is characterized by fine-grained pyrite-rich ore (Table 3, Fig. 2). There is a weak pyrite grain-shape foliation throughout the sample (Fig. 8i). Pyrite grains are well rounded with pyrite–pyrite boundaries irregular and often "sutured" in appearance (Figs. 3i, j and 8e). The majority of pyrite grains are surrounded by a thin sliver of either pyrrhotite or chalcopyrite (Fig. 3j). Few inclusions are present within pyrite grains and brittle fracturing is uncommon. OC images (Fig. 8e) indicate widespread internal gray-scale variation, and EBSD analysis shows lattice rotation occurred either about a single or two <100> axes. Cumulative misorientation in pyrite grains is typically ~4° (Table 3; Fig. 5) and low-angle (~2°) subgrain boundaries are common (Fig. 8f). The neighbor-pair misorientation angle histogram is dominated by a low-angle (~2°) boundary peak almost three times higher than the theoretical random distribution peak at ~60° while random-pair misorientations appear random (Fig. 8g). There is evidence for a weak CPO defined by lattice alignment to a <111> crystallographic axis (Fig. 9).

Discussion

This discussion aims to address three main questions which have arisen during investigation of the Røros specimens in this study. Firstly, what are the relationships between the

primary and/or deformation textures preserved within pyrite in the individual Røros ore deposits? Secondly, which deformation mechanisms have operated at the perceived peak metamorphic conditions, and do these correspond with the preserved pyrite textures? Thirdly, what do textural features such as grain-size modification, brittle-fracturing, and 120° triple-junction development reveal about an ore deposit's deformation and metamorphic history?

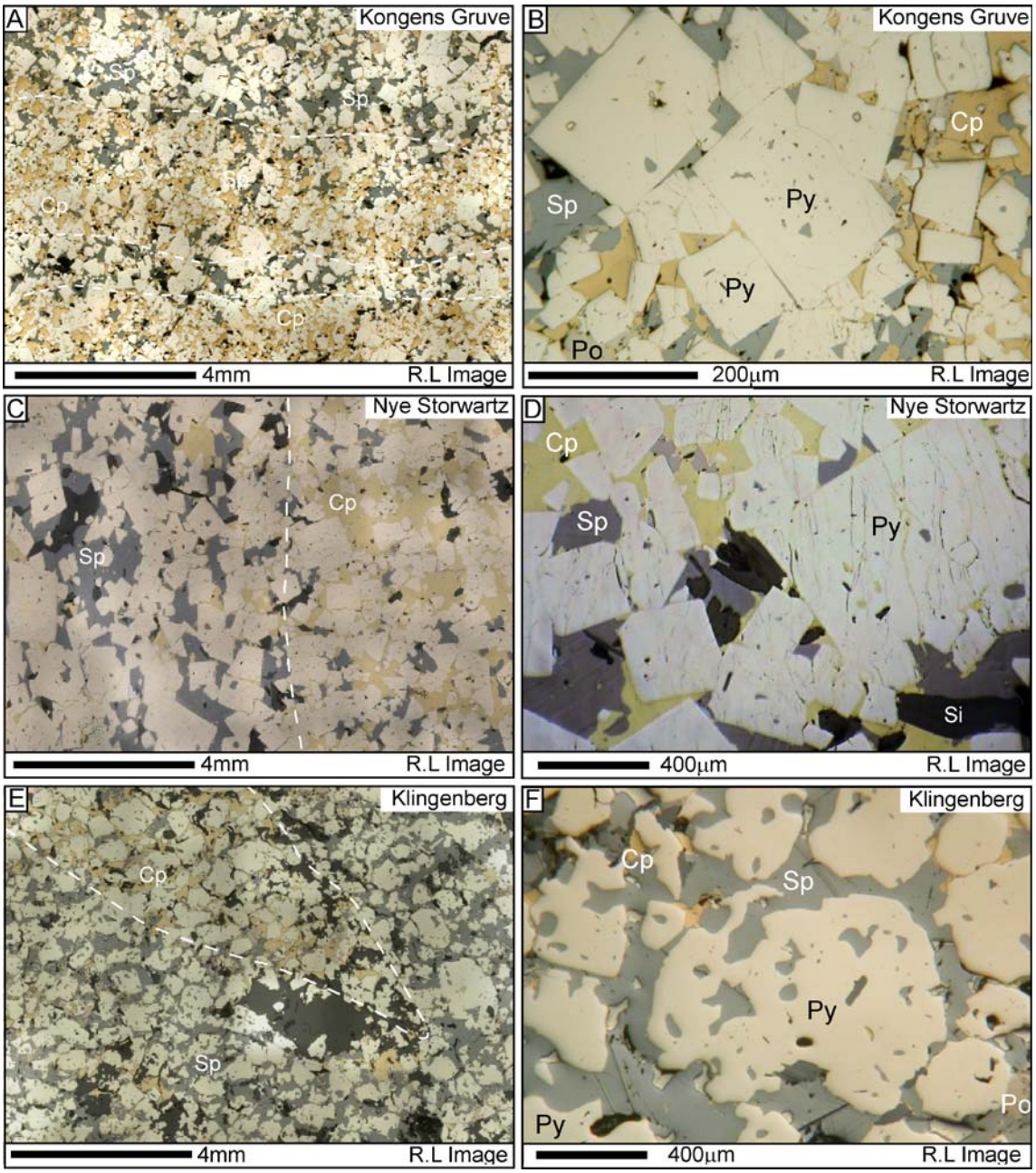

Fig. 3 Reflected-light photomicrographs of all of the samples discussed in this study: pyrite (*Py*), chalcopyrite (*Cp*), sphalerite (*Sp*), pyrrhotite (*Po*) and silicates (*Si*) **a** Compositional and grain-size layering at Kongens Gruve **b** Equant pyrite blasts with potential dissolution pyrite-pyrite boundaries at Kongens Gruve. Rounded inclusions of sphalerite are obvious in the larger pyrite grains **c** Compositional layering between sphalerite and chalcopyrite-rich domains at Nye Storwartz. **d** Brittle fractures, filled with slivers of chalcopyrite, in euhedral pyrite blasts at Nye Storwartz. Inclusions of sphalerite are also obvious in many of the pyrite grains **e** Compositional lensing defined by chalcopyrite abundance at Klingenberg. **f** Embayed anhedral pyrite grains at Klingenberg highlighting the irregular nature of pyrite porphyroblasts and the abundance of large inclusions of the surrounding sulfides. **g**/**h** Images of Guldals Grube pyritic ores highlighting the relationship between pyrite grains and the surrounding phases. **i**/**j** Images of Godthåp ore highlighting the relationship between pyrite grains and the surrounding phases as well as a possible grain shape foliation (*highlighted* in **c**) and the irregular appearance of pyrite grain boundaries, *highlighted* with *arrows* in **d**

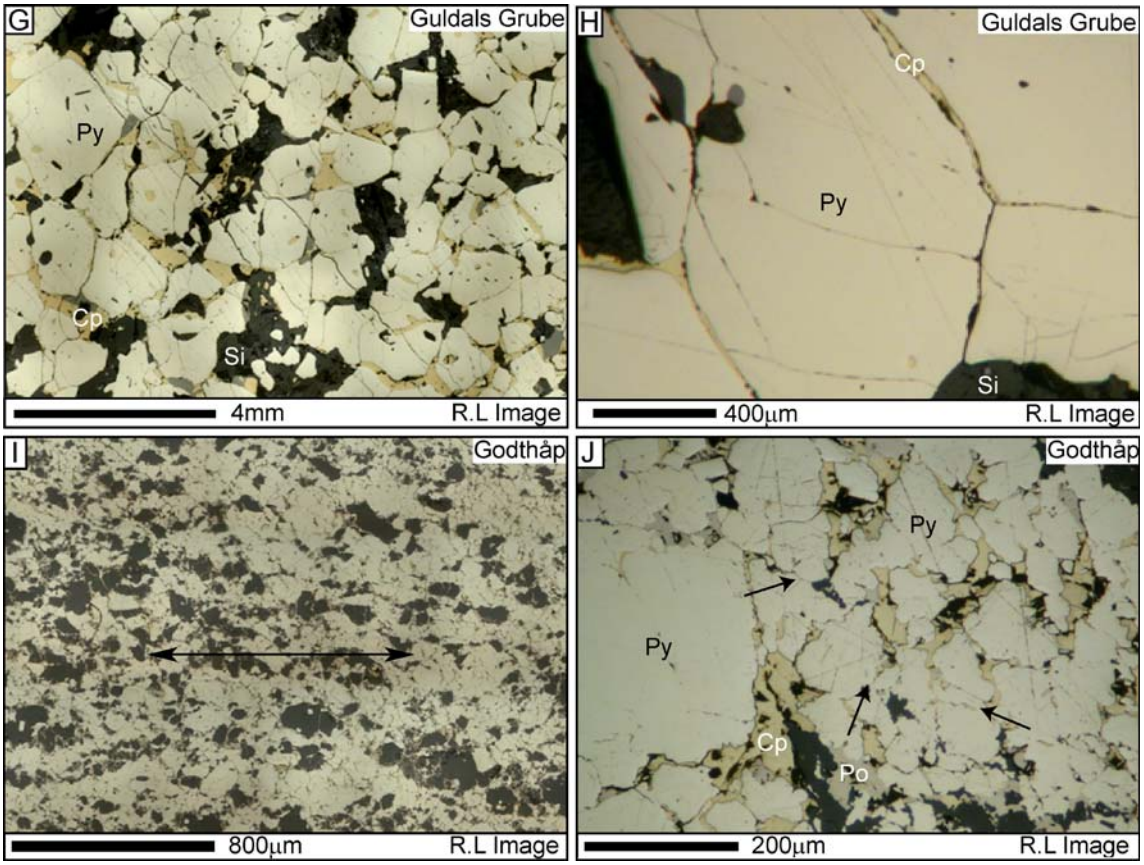

Fig. 3 (continued)

Pyrite morphology variation

Pyrite grain shape

There are substantial differences in pyrite grain sizes and shapes between the samples from individual ore deposits (Figs. 3, 8). The majority of samples contain relatively equant pyrite grains with straight, sharp pyrite–pyrite contact boundaries, however, some preserve more unusual grain shapes. Pyrite grains at Godthåp have irregular, "sutured" boundaries (Figs. 3i, j and 8) with some evidence for micron-scale bulging. Barrie et al. (2007) reported similar textures in experimentally deformed pyrite samples and concluded that they most likely represented recrystallization processes, specifically bulging.

Pyrite grains from the Klingenberg specimens also preserve irregular boundaries; however, these preserve an "embayed" rather than "sutured" texture resulting in a very elongate, "irregular" appearance of grain boundaries in many of the pyrite grains (Figs. 3e, f and 7). This suggests that these two textures have formed as a result of different processes and while Godthåp may represent recrystallization processes, there is no evidence for this at Klingenberg. These "embayment" textures have also been reported from the upper amphibolite facies Bleikvassli deposit (Fig. 1a) further north of the suite of ore deposits investigated in this study (Craig and Vokes 1992).

Assuming the system was chemically closed, two possible modes of origin of the "embayed" pyrite texture in the Klingenberg deposit are:

1. Disequilibrium between pyrite grains and the surrounding sulfide phases during metamorphism resulted in pyrite being replaced by the surrounding phases.
2. Pyrite grains underwent rapid growth during prograde metamorphism, overprinting, engulfing, and replacing the surrounding sulfide phases resulting in large inclusions, embayed boundaries, and a heterogeneous morphology.

While there is no direct evidence against the first mechanism, the fact that pyrite is clearly stable across the range of metamorphic conditions experienced in the Røros deposits make this mechanism unlikely. Craig and Vokes (1992) suggest that similar embayment textures at the

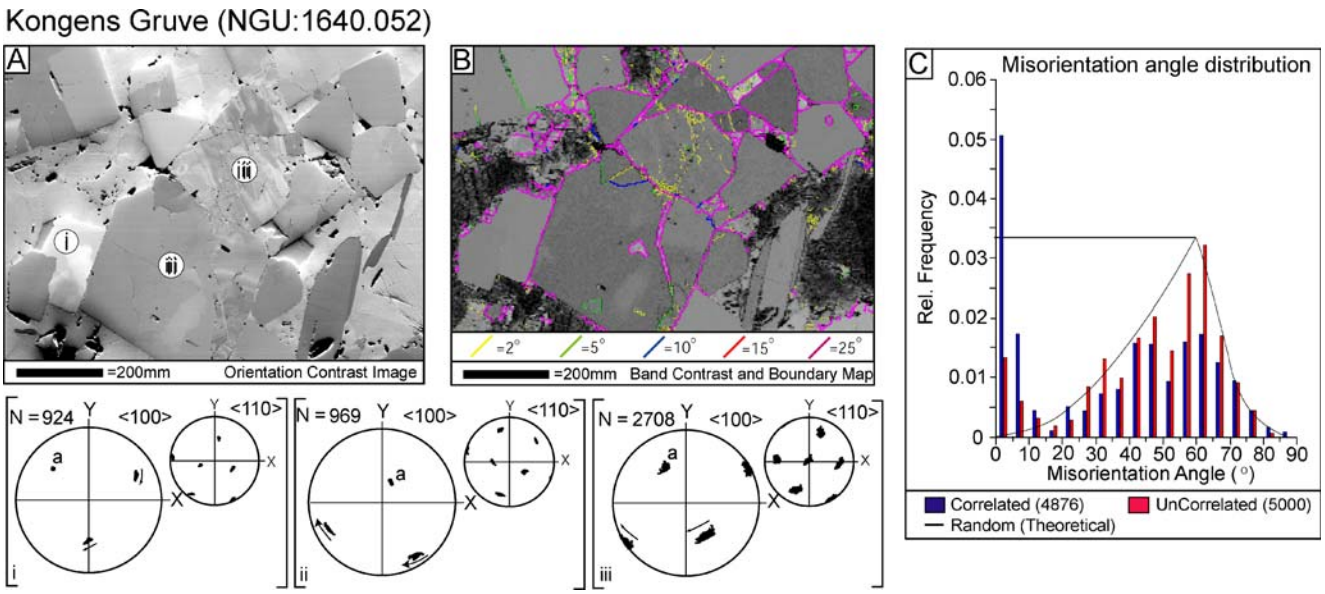

Fig. 4 EBSD data for Kongens Gruve **a** Orientation contrast image with pole figures for selected grains (*i, ii, iii*), lattice rotations are *highlighted* in the pole figures. **b** EBSD band contrast image overlain with misorientation boundaries. **c** Misorientation angle distribution for all pyrite grains mapped at Kongens Gruve. Correlated data are from adjacent pairs of pyrite grains, uncorrelated data represent randomly chosen pairs of non-adjacent grains. The misorientation angle distribution of a theoretically random distribution of pyrite grains is shown for reference

Bleikvassli ore deposit in Norway (Fig. 1a) formed at least partly due to the presence of an abundance of softer matrix sulfide phases. However, the Nye Storwartz and Kongens Gruve ores contain a similar abundance and composition of minor phases to Klingenberg (Table 2; Fig. 3), yet both of these deposits are dominated by equant pyrite crystals with no obvious embayment of pyrite-grain boundaries. This suggests that rapid pyrite growth is a more likely explanation for the textures preserved at Klingenberg reflecting either higher temperatures and/or more rapid heating with the onset of prograde metamorphism. Therefore, while this texture is likely to have developed due to rapid growth, it is likely to have been enhanced by the nature of the matrix sulfide phases (Craig and Vokes, 1992). An abundance of softer sulfide (chalcopyrite, sphalerite) or silicate (chlorite) phases surrounding pyrite grains will allow relatively unrestricted pyrite grain growth (Cook, 1996), whereas specimens dominated by pyrite and pyrite–pyrite contacts will not have the same growth freedom.

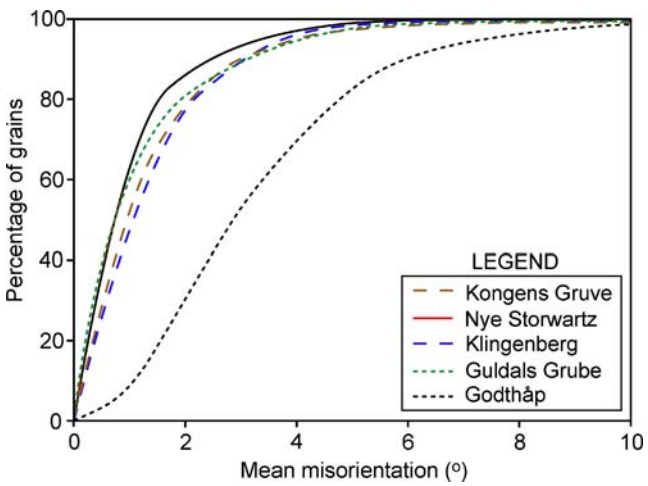

Fig. 5 Cumulative frequency histogram plotting mean lattice misorientation within individual pyrite grains against the total percentage of grains within each sample

Pyrite grain size

There are four main processes which can affect the grain size in deformed and/or metamorphosed sulfide ore deposits:

1. Initial grain-size developed during primary precipitation (Barrie et al. 2009).
2. Grain-size increase due to growth of crystals during prograde metamorphism (Vokes 1969; McClay and Ellis 1983; Cook 1996).
3. Grain-size reduction during postmetamorphic recovery and/or recrystallization processes (Barrie et al. 2007).
4. Grain-size reduction as a result of brittle behavior and cataclasis of pyrite grains.

There is little evidence that the last two processes have significantly influenced the grain size preserved within the specimens investigated with the exception of the Godthåp deposit. Previous work in the Norwegian Caledonides (Vokes 1976; Craig and Vokes 1992), as well as other

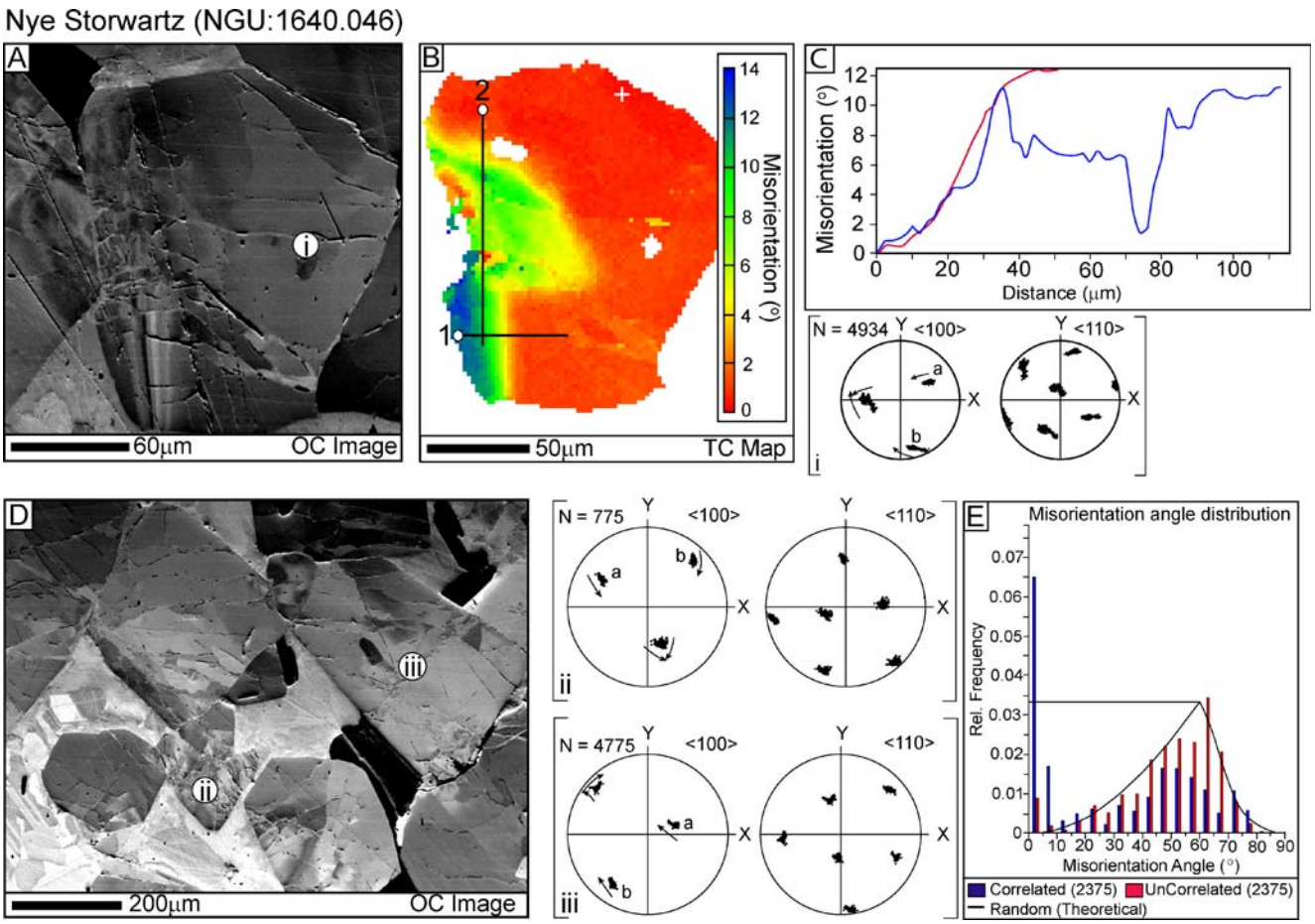

Fig. 6 EBSD data for Nye Storwartz. **a** Orientation contrast image with pole figure (*i*) for the pyrite grain; lattice rotations are *highlighted* on pole figure. **b** Texture component map highlighting misorientation changes across the pyrite grain. **c** Cumulative misorientation profiles for the transects shown (*i*) in **a**. **d** Orientation contrast image of pyrite grains with pole figures (*ii*, *iii*) included; lattice rotations are *highlighted* on the pole figures. **e** Misorientation angle distribution for pyrite grains in all of the grains mapped at Nye Storwartz. Correlated data are from adjacent pairs of pyrite grains; uncorrelated data represent randomly chosen pairs of nonadjacent grains. The misorientation angle distribution of a theoretically random distribution of pyrite grains is shown for reference

sulfide ore deposits (Mookherjee 1976; McClay and Ellis 1983), suggests a general trend of increasing grain size with increasing metamorphic grade. In the Røros deposits, there is the suggestion of a similar trend with grain size increasing from southwest (Kongens Gruve) to northeast (Guldals Grube). However, the most northeasterly deposit, Godthåp, has the finest pyrite grain size (~30 μm) of all of the ore deposits investigated. Indeed, Guldals Grube and Godthåp are the most closely related deposits in terms of location, host lithology, and likely metamorphic grade but grain size differs by almost an order of magnitude (~280 μm and ~30 μm, respectively, Figs. 1b and 2).

Godthåp is a very minor deposit in the sequence, and the grain size of the pyrite is anomalously fine-grained when compared with the other ore deposits investigated (Fig. 2). Pyrite grains at Godthåp also contain the only evidence for recrystallization processes via possible grain boundary bulging (Fig. 8e). This evidence coupled with the presence of a greater proportion of pyrrhotite forming the matrix sulfide material suggests this deposit may have undergone shearing along the ore horizon during deformation. The presence of pyrrhotite in itself does not imply shearing; however, this process is readily reported to take place along pyrrhotite-dominant ore horizons with the tectonoclastic ores of the Sulitjelma ore field, Norway showing this in quite spectacular fashion (Cook et al. 1993; Cook 1996). This potential movement in the Godthåp deposit may well explain why recrystallization processes, and hence, a much finer grain size (Fig. 2) has developed during deformation and metamorphism in this deposit but not in the others particularly Guldals Grube.

Grain-size defined foliations (Fig. 3) are apparent in samples from Nye Storwartz, Kongens Gruve, and Klingenberg as well as other ore deposits in the Norwegian Caledonides (Craig and Vokes 1992). This layering may indicate a contribution to final grain size from initial

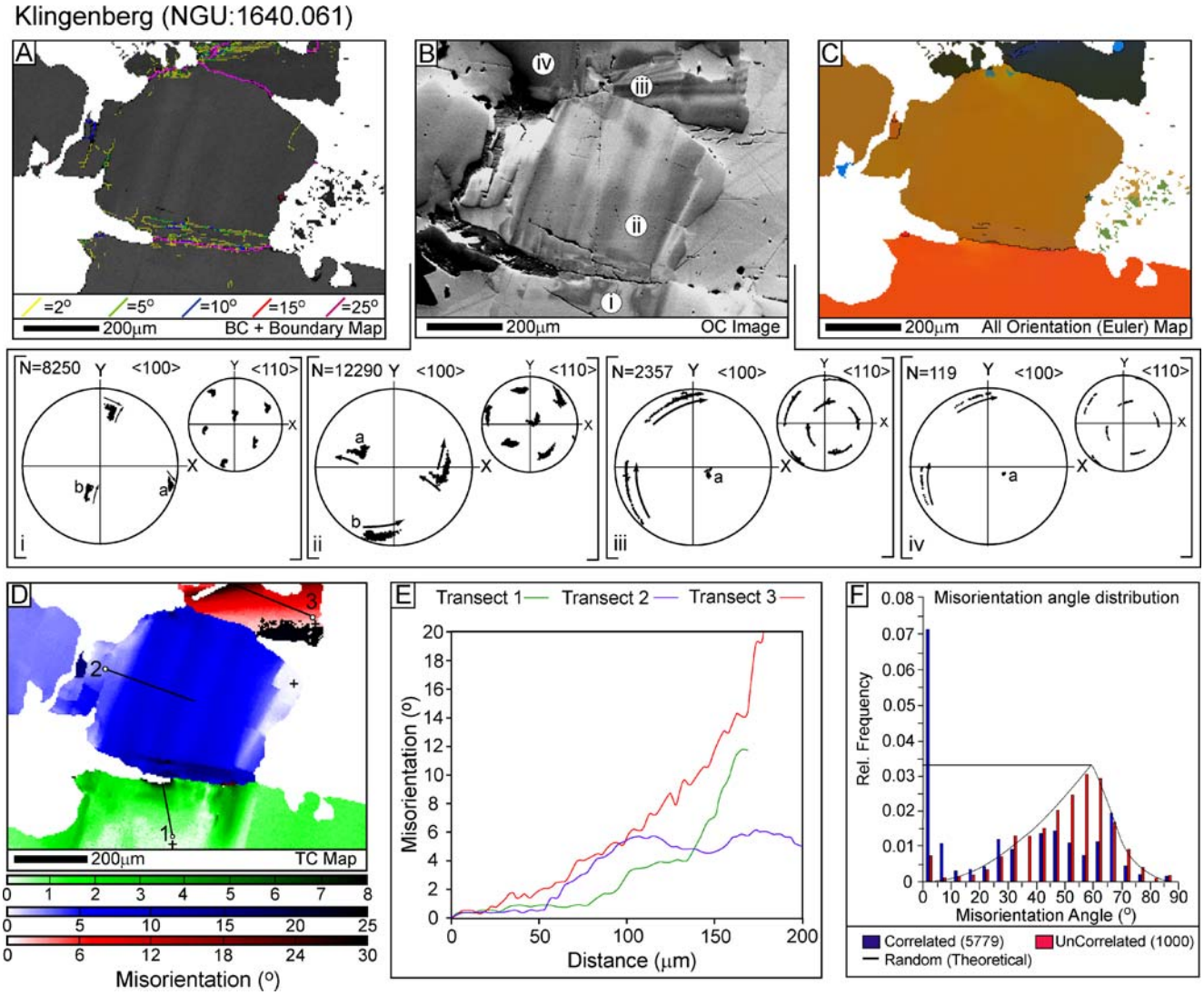

Fig. 7 EBSD data for Klingenberg **a** EBSD map of band contrast overlain by misorientation boundaries. **b** Orientation contrast image with pole figures for selected grains: grain *iii* and *iv* preserve rotation about a single <100> axis, and grains *i* and *ii* preserve rotation about two separate <100> axes; lattice rotations are *highlighted* on the pole figures. **c** EBSD Euler-angle map of all orientations within each pyrite grain; note subtle *variations in color* representing changes in crystallographic orientation within grains. **d** Texture component map highlighting misorientation changes within the three main pyrite grains. **e** Cumulative misorientation profiles for the three transects shown in **d**. **f** Misorientation angle distribution for all pyrite grains mapped at Klingenberg. Correlated data are from adjacent pairs of pyrite grains; uncorrelated data represent randomly chosen pairs of nonadjacent grains. The misorientation angle distribution of a theoretically random distribution of pyrite grains is shown for reference

variations in primary pyrite grain size (Barrie et al. 2009). However, because all of the ore deposits have also experienced deformation and metamorphism, there is no way to quantify primary grain size, which is a problem. Thus, while coarse-grained pyrite often preserves textures associated with blastesis, indicating grain-size increase during metamorphism (Figs. 3, 4), the absence of evidence for the premetamorphic grain size makes quantification of the effects impossible. Pyrite growth and grain size as well as possibly degree of reequilibration will also be heavily influenced by the enclosing minerals and their relative abundances on the millimeter- to meter-scale, which ultimately define the rheology of the rock. Indeed, such factors may be more important than the local stress/strain regime or the overall pressure and temperature conditions of metamorphism. Coexisting sulfide minerals and gangue phases are both critical: Pyrite in a matrix of abundant pyrrhotite and/or chalcopyrite will behave differently to pyrite in an ore where there is only a very small amount of matrix of ductile sulfides between grains (Marshall and Gilligan 1987).

The literature includes described examples of pyrite that either grew uninhibited to centimeter-size proportions (Cook 1996) or alternatively was replaced by a more ductile phase resulting in the preservation of pyrite relicts

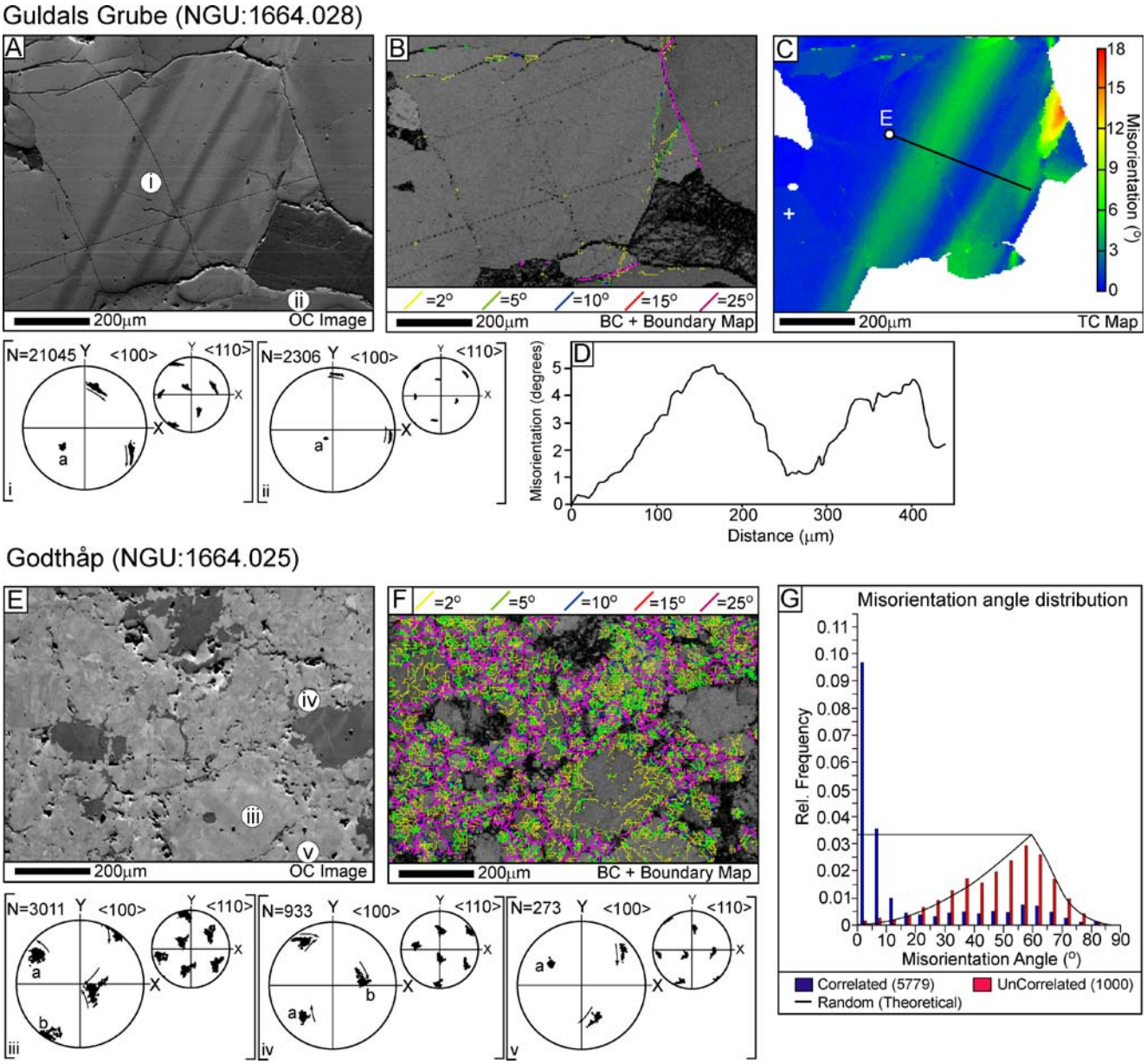

Fig. 8 EBSD data for Guldals Grube and Godthåp samples. **a** Orientation contrast image with pole figures for selected grains (*i* and *ii*); lattice rotations are *highlighted* on the pole figures. **b** EBSD band contrast image overlain with misorientation boundaries. **c** Texture component map highlighting misorientation changes **d** Cumulative misorientation profile across the transect shown in **c**. **e** Orientation contrast image with pole figures for selected grains (*iii*, *iv*, and *v*); lattice rotations are *highlighted* on pole figures. **f** EBSD band contrast image overlain with misorientation boundaries. **g** Misorientation angle distribution for all pyrite grains mapped at Godthåp. Correlated data are from adjacent pairs of pyrite grains; uncorrelated data represent randomly chosen pairs of nonadjacent grains. The misorientation angle distribution of a theoretically random distribution of pyrite grains is shown for reference

(Craig and Vokes 1993). Similarly, it is reasonable to assume that pyrite growth will be less inhibited by a matrix of softer chlorite in comparison with a more rigid quartz gangue. The matrix material of the ore would, of course, change during metamorphism not only through formation of the metamorphic gangue mineral assemblages (or several stages thereof during the prograde and retrograde cycles) but also possibly through formation of pyrrhotite at the expense of pyrite (Craig and Vokes 1993) or vice versa and the widespread replacement or "corrosion" of pyrite by the more ductile sulfide phases.

In addition, to all of these changes remobilization may also occur—physical transfer of sulfide-forming materials from one location within the orebody to another (internal remobilization) or external into the wall rock (external remobilization; Marshall et al. 2000). The metamorphic/deformational episode may also involve sulfidation or desulfidation of the ore (Spry 2000) influencing the

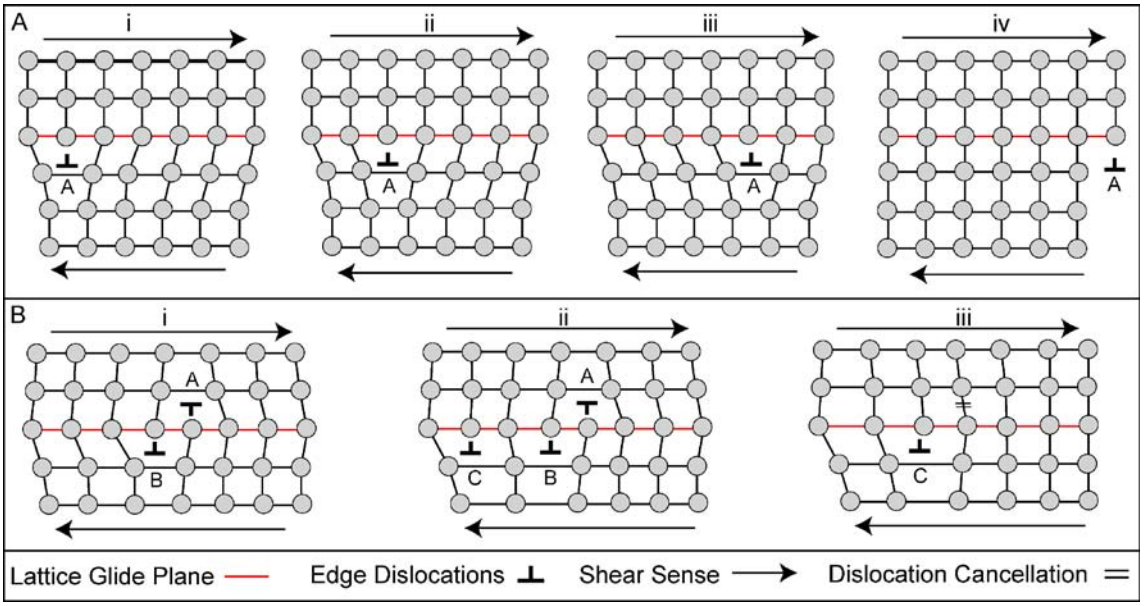

Fig. 9 **a** Example of a typical edge dislocation propagating to the right along a glide plane and exiting a crystal (*i–iv*) without being obstructed by any obstacles or "opposite" edge dislocations along the glide plane. **a**, **b** Example of edge dislocations propagating along a glide plane in "opposite" directions and meeting to form an obstruction, thus, "locking" propagation of any further dislocations along the glide plane (*i–ii*). By stage *iii* dislocation, **b** has "climbed" up into a higher lattice plane, canceling dislocation (**a**), thus, allowing glide to continue. The distortion of the lattice is schematic and exaggerated in both **a** and **b** (modified after Davis and Reynolds 1996)

mineralogical evolution. These factors will, to varying degrees, have influenced the morphological–textural appearance of the ores as seen today even if discussion of their contributions in each of the studied deposits is beyond the scope of this paper. It is likely, however, that the currently preserved pyrite grain-size in each of the ore deposits is not simply an indicator of increasing metamorphic grade but instead reflects a complex interplay between growth processes, premetamorphism inherited grain-size, gangue mineralogy, the influence of the stress regime during growth as well as grain-size reduction, and remobilization processes.

Deformation textures

Brittle behavior

Brittle deformation is a common texture in the Norwegian stratabound ore deposits (Vokes 1969; Vokes 1976; Marshall and Gilligan 1987). The obvious evidence for brittle fractures has led many authors to suggest that cataclasis is the predominant deformation mechanism affecting pyrite (Vokes 1969; Marshall and Gilligan 1987; Cook 1993). However, all of the specimens investigated have experienced plastic deformation as evidenced by lattice distortion and misorientation (Fig. 5), which must predate brittle deformation events. Thus, it is likely that brittle deformation occurred after peak metamorphic conditions at lower temperatures, conditions at which the softer sulfides remained ductile and flowed into these fractures (Marshall and Gilligan 1987, 1993; Bailie and Reid 2005).

Brittle behavior in the ores will not only be affected by evolving temperature during metamorphism but also by rates of fluid flow. This process will affect the individual ore deposits to varying degrees and is dependent upon a number of factors including: ore deposit size and temperature of metamorphism (Etheridge et al. 1983; Cox 1987; McCaffrey et al. 1999). Brittle deformation may also be influenced by the differences in abundance and composition of the matrix sulfide phases. Guldals Grube (Fig. 3g, h) which contains the lowest proportion of softer sulfide phases (Table 2) contains the most pyrite–pyrite impingement contacts and preserves the most extensive fracturing. In contrast, Klingenberg contains the greatest abundance (50%) of softer sulfide phases (Table 2) and shows very few pyrite–pyrite impingement contacts and fracture development appears almost absent.

Annealment textures

Annealment or "foam" textures occur when grain boundaries develop characteristic 120° triple junctions and are thought to indicate grains achieving textural equilibrium through recrystallization at high temperature in the absence of oriented deformation (McQueen 1987; Craig and Vokes 1992; Mücke and Younessi 1994; Craig et al. 1998; Craig 2001). Such textures are prominent at Guldals Grube (Fig. 3h) and, to a lesser extent, Gothåp, though OC images

and EBSD analysis indicate that the pyrite grains have significant internal plastic strains (Fig. 8). The presence of plastic deformation within triple-junction pyrite grains therefore suggests that these "apparent" foam textures are not indicative of equilibrium recrystallization. Indeed, it is more likely that these textures represent grain boundary adjustment with combined dissolution and syntaxial growth at the grain boundaries producing the characteristic triple junctions but leaving the volume of the grain unaffected (Barrie et al. 2007).

Plastic deformation

With the exception of a few elongate grains, there is little suggestion from reflected light or BSE imaging for plastic deformation. However, it is apparent from the results above utilizing OC imaging coupled with EBSD analysis that plastic deformation is apparent in all of the ore deposits investigated. This plastic deformation has involved the pyrite lattice being misoriented by rotation about one or two <100> axes (Figs. 4, 6, 7, 8) with cumulative misorientations up to ~30° (Table 3). Low-angle (~2°) subgrain boundaries, widespread at Godthåp, indicate that both dislocation glide and associated climb recovery mechanisms have operated. The poor development of dislocation walls, other than at grain boundaries or impingement zones, as evident at Klingenberg (Fig. 7) and Guldals Grube (Fig. 8), suggest dislocation glide has been more important than dislocation creep. Misorientation profiles through pyrite grains highlight the operation of glide with grains preserving continuous, steady changes in lattice misorientation (Figs. 7e, 8c) at increments limited by the ~1° resolution of the EBSD analysis.

Dislocation glide operates freely within deforming crystals when dislocations can glide along the lattice plane without becoming "locked" by obstacles or other "opposite" dislocations (Fig. 9a) along the glide plane (Cox 1987; Passchier and Trouw 2005). When dislocation "locking" occurs, dislocations develop tangles and continued glide becomes either inhibited or impossible and strain hardening occurs (Fig. 9b). In order for dislocation glide to continue, recovery is essential, and this is generally accommodated by dislocation climb whereby the dislocation bypasses the blockage by moving into an adjacent lattice plane resulting in formation of a new low-angle (~2°) subgrain boundary (Fig. 9b). Dislocation walls have only been found near grain boundaries, and particularly impingement zones, in most of the specimens investigated suggesting that where pyrite grains impinge upon one another, deformation stresses increase, and dislocation creep is favored over glide mechanisms (Cox 1987; Barrie et al. 2008).

Therefore, two plastic deformation mechanisms were common in the pyrite grains at Røros; the cores of pyrite grains deformed by glide mechanisms while grain boundary regions and impingement zones deformed via dislocation creep. The change from dislocation glide to creep is generally associated with increasing temperature, but other factors such as stress magnitude and strain rate are also important (McClay and Ellis 1983). It is unlikely that temperature varied significantly within pyrite grains, but stress magnitude and strain rate could very likely be higher at pyrite–pyrite grain contact regions and thus explain the change in deformation mechanism at grain margin areas (Fig. 7a).

Crystal-preferred orientations

A major result of dislocation glide processes in many polycrystalline materials is the development of a CPO (Cox 1987; Zhang and Wilson 1997; Vernooij et al. 2006). A number of studies of dislocation–glide mechanisms and crystallographic fabrics have discussed CPO development in sulfide ores (McClay and Ellis 1983; Henning-Michaeli 1985; Siemes et al. 1993; Jansen et al. 1998).

In the Røros ore deposits, all of the samples preserve random bulk CPOs, apart from Godthåp, which has a potentially very weak <111> CPO. However, CPOs of this strength are very subjective (Siemes et al. 1993; Barrie et al. 2007) and may. in fact, represent a random orientation of pyrite crystals (Fig. 10). Previous work (Barrie et al. 2007, 2008) has suggested that CPO development in polycrystalline pyrite is unlikely due to the number of independent slip-systems which can potentially be active during deformation. If the fabric preserved at Godthåp does represent a weak <111> CPO, then there are two possible processes that could be responsible:

1. This fabric represents a unique set of deformation conditions, potentially shearing along the ore horizon previously suggested, which promoted a <111> CPO of pyrite grains.
2. This fabric represents a relic of an initial primary orientation of the pyrite crystals (Freitag et al. 2004) which has been weakened during subsequent deformation of the ore.

Considering the samples studied by Barrie et al. (2007), experienced strains of up to ~40% without any apparent CPO development, it is difficult to envisage conditions during natural deformation which would result in formation of a CPO. However, the suggestion that shearing may have taken place at Godthåp coupled with the presence of a shape-preferred orientation of the pyrite grains means that this mechanism cannot be ruled out as potentially responsible. The suggestion of possible remnant depositional layering in some of the specimens investigated (Figs. 3 and 8) coupled with the general lack of CPOs developing in deformed pyrite suggests the latter scenario is the most likely; though, it must

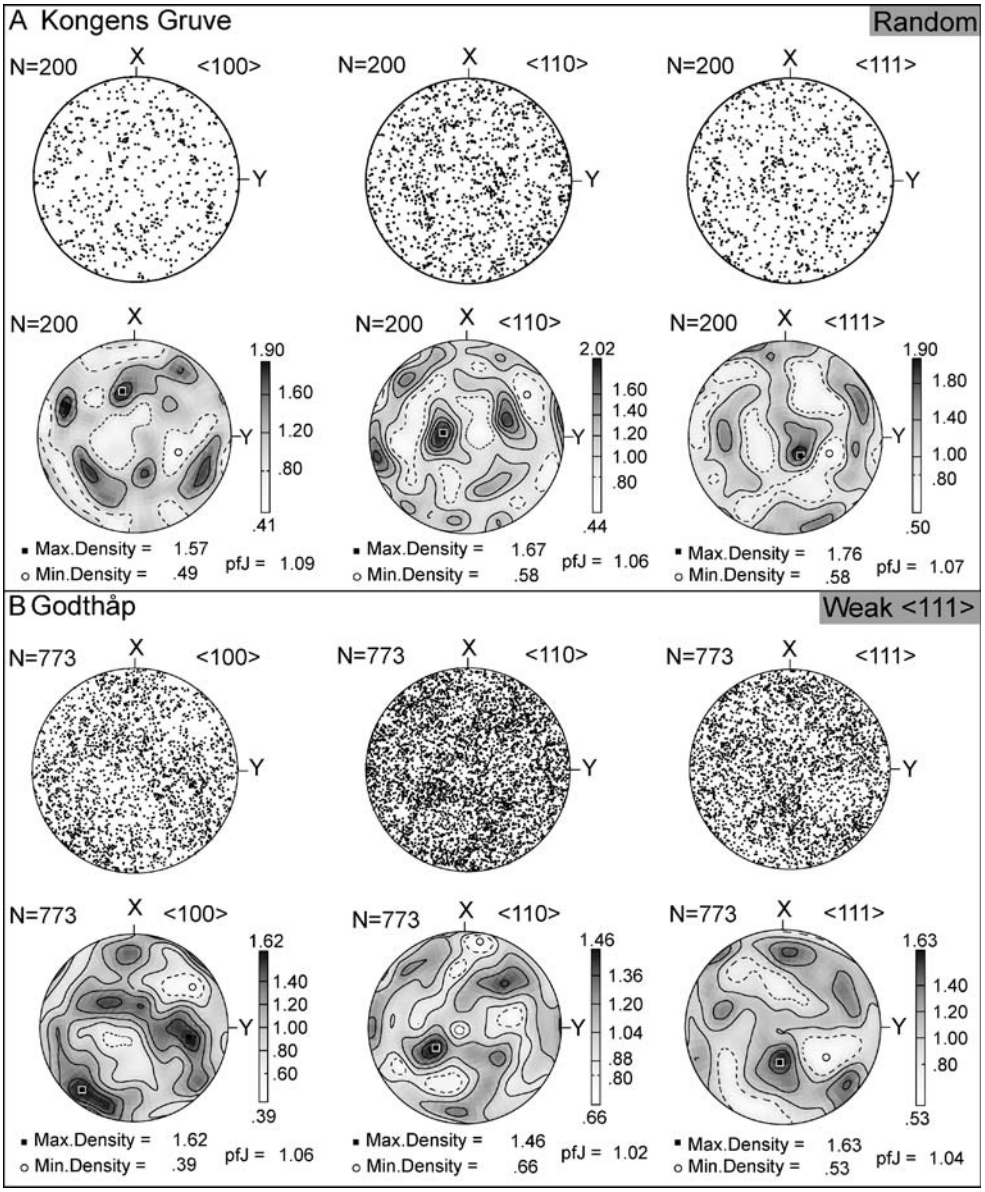

Fig. 10 Scatter and contoured one-point-per-grain pole figures **a** Kongens Gruve showing a random or "uniform" distribution of grains. **b** Godthåp showing a weak CPO developed about a <111> or possibly a <110> axis

be emphasized that the CPO pattern preserved is likely to be more subjective than real.

Deformation history

While the CPO at Godthåp (Fig. 10) and the grain size and compositional changes in the samples (Figs. 3 and 8) may represent remnant primary layering, there is little evidence for definite primary textures in any of the Røros ore deposits investigated. There are, in all of the specimens investigated, few textures unequivocally representative of the premetamorphic phase of ore deposit evolution. Although grain size and compositional layering (Fig. 3) is apparent in many of the samples establishing this as definitively predeformational is contentious at best (Vokes, 1968; Bryhni and Andreasson 1985; Ihlen et al. 1997). The textures preserved in all of the specimens in this study suggest an overall history of growth of pyrite grains during prograde metamorphism, coupled with plastic deformation of pyrite at peak metamorphic conditions, followed by local brittle deformation either during retrograde cooling or increased strain conditions. There is some evidence for the development of ~120° triple junctions at grain boundaries together with evidence for brittle fracture of pyrite associated with flow of softer sulfide minerals into the fractures. A generalized deformation history for the pyritic ores of the Røros district would be as follows:

1. Largely unknown primary textures resulting from the local depositional environment.

2. Prograde metamorphism resulting in rapid growth of pyrite grains in Klingenberg with slower growth in the other ore deposits resulting in the observed inclusion and embayment relationships in the pyrite grains at Klingenberg.
3. Peak metamorphic conditions at greenschist–amphibolite facies associated with significant strain resulting in plastic deformation of the pyrite crystals dominated by glide except near pyrite–pyrite contacts where creep occurred.
4. Local reequilibration of grain boundaries to give foam textures without removing plastic strains from pyrite grains.
5. Cataclasis and "pulverization" of pyrite grains during a change in the prevalent deformation/metamorphic conditions. These mechanisms would become dominant either during the effects of lower temperatures during retrograde cooling or through a change in the deformation regime resulting in increased strains. Temperatures at this stage must still have been sufficiently high for continued remobilization of the sphalerite and chalcopyrite phases which flowed into the fractures developed in the now rigid pyrite.

This kind of study is still in its relative infancy, and the work reported throughout is somewhat preliminary in character given the relatively small number of specimens, the choice of specimens, and the bias in their selection. Use of EBSD to understand pyrite deformation mechanisms is, however, an important and valuable technique that can assist with correlation of observed assemblages, textures, and fabrics with discrete episodes of deformation or multiple overprinting events (Boyle et al., 1998; Barrie et al. 2007, 2009). The method therefore has major implications for deciphering discrete generations of pyrite. This could carry relevance in cases where there are clearly discrete generations of pyrite not only in metamorphosed VMS ores but also, for example, in "orogenic gold" deposits. Internal structures in pyrite, especially when coupled with microchemical analysis, also carry implications for ore economics or process mineralogy if the pyrite in question is also a significant carrier of invisible gold (Cook and Chryssoulis 1990; Cook et al. 2009) as well as for understanding release of deleterious elements into the environment during sulfide breakdown.

Conclusions

The Røros orefield contains a suite of massive pyritic ore deposits, which preserve different grain sizes, compositions, and textures. Reflected light observations indicate that foam textures overprinted by brittle fracturing are dominant, which classically would suggest annealing of the ores at peak metamorphic conditions followed by brittle deformation during cooling and perhaps exhumation. However, combined orientation contrast imaging and EBSD analysis indicate that pyrite in all of the ore deposits was predominantly affected by plastic deformation regardless of grain size or inferred metamorphic grade. The apparent foam textures present in some of the ore deposits are likely to represent localized grain boundary readjustments in which some pyrite grains must have been partially dissolved and adjacent pyrite grains syntaxially overgrown to give 120° triple junctions without any annealing of grain interiors.

Plastic deformation of pyrite involved a combination of dislocation glide within pyrite grain cores and dislocation creep at grain boundaries except in Godthåp where pyrite deformation appears to be entirely due to dislocation creep. This plastic deformation did not produce bulk CPOs except for a possible weak <111> CPO at Godthåp, which is potentially either primary in origin or related to shearing. There is no systematic correlation between changes in grain size and metamorphic grade implied from geographical location. Current pyrite grain sizes are likely to have developed as a result of a complex interplay of many processes involving primary precipitation, metamorphic growth, grain-size reduction via recrystallization (exclusively at Godthåp), abundance, and composition of the minor phases and remobilization.

Finally, this work provides a warning for the interpretation of sulfide textures. Previous work has suggested pyrite was rigid and brittle in the deposits at Røros (Rui and Bakke 1975); however, this study indicates plastic strain is present in all of the deposits, and the obvious brittle deformation is a later effect developed after peak metamorphic conditions. Reflected light microscopy and backscatter electron imaging are still important tools for studying sulfide textures, but they are not, by themselves, adequate for documenting plastic deformation in opaque cubic minerals.

Acknowledgments This paper which has been funded by a University of Liverpool studentship forms part of the PhD of C. D. B. John Gilleece is thanked for preparation of the Nye Storwartz specimens. Some samples in this study derive from the Geological Survey of Norway ore database; access to the collection by one of the authors (N. J. C.) at the time of his employment there is gratefully acknowledged. Two anonymous reviewers and the editor Pat Williams are thanked for their constructive suggestions on alterations to the manuscript.

References

Allen RL, Weihed P, Blandell D, Crawford T, Davidson G, Galley A, Gibson H, Hannington M, Herrington R, Herzig P, Large R, Lentz D, Maslennikov V, McCutcheon S, Peter J, Tornos F

(2002) Global comparisons of volcanic-associated massive sulphide districts. Geological Society Special Publication 204:13–37

Atkinson BK (1975) Experimental deformation of polycrystalline pyrite: effects of temperature, confining pressure, strain rate and porosity. Economic Geology 70:473–487

Bailie RH, Reid DL (2005) Ore textures and possible sulphide partial melting at Broken Hill, Aggeneys, South Africa I: petrography. S Afr J Geol 108:51–70

Barrie CD, Boyle AP, Prior DJ (2007) An analysis of the microstructures developed in experimentally deformed polycrystalline pyrite and minor sulphide phases using electron backscatter diffraction. J Struct Geol 29:1494–1511

Barrie CD, Boyle AP, Cox SF, Prior DJ (2008) Slip systems in pyrite: an electron backscatter diffraction (EBSD) investigation. Mineral Mag 72:1147–1165

Barrie CD, Boyce AJ, Boyle AP, Williams PJ, Blake K, Ogawara T, Akai J, Prior DJ (2009) Growth controls in colloform pyrite. Am Mineral 94:415–429

Bjerkgård T, Sandstad JS, Sturt BA (1999) Massive sulphide deposits in the South-Eastern Trondheim Region Caledonides, Norway: a review. In: Stanley CJ (ed) Mineral deposits: processes to processing: proceedings of the Fifth Biennial SGA meeting. A. A. Balkema, London

Boyle AP, Prior DJ, Banham MH, Timms NE (1998) Plastic deformation of metamorphic pyrite: new evidence from electron-backscatter diffraction and forescatter orientation-contrast imaging. Miner Deposita 34:71–81

Brown D, McClay KR (1993) Deformation textures in pyrite from the Vangorda Pb-Zn-Ag deposit, Yukon, Canada. Mineral Mag 57:55–66

Bryhni I, Andreasson P-G (1985) Metamorphism in the Scandinavian Caledonides. In: Gee DG, Sturt BA (eds) The Caledonide orogen, Scandinavia and related areas. Wiley, London, pp 763–781

Bugge JAW (1978) In: Bowie SHU, Kvalheim A, Haslam HW (eds) Mineral deposits of Europe: volume 1 Northwest Europe. Institution of Mining and Metallurgy/Mineralogical Society, London, pp 199–249

Castroviejo R (1990) Gold ores related to shear zones, west Santa Comba–Fervenza area (Galicia, NW Spain)—a mineralogical study. Miner Deposita 25:42–52

Cook NJ (1993) Conditions of metamorphism estimated from alteration lithologies and ore at the Bleikvassli Zn–Pb–(Cu) deposit, Nordland, Norway. Nor Geol Tidsskr 73:226–233

Cook NJ (1996) Mineralogy of the sulphide deposits at Sulitjelma, northern Norway. Ore Geol Rev 11:303–338

Cook NJ, Chryssoulis SL (1990) Concentrations of invisible gold in the common sulfides. Can Mineral 28:1–16

Cook NJ, Ciobanu CL, Mao JW (2009) Textural control on gold distribution in As-free pyrite from the Dongping, Huangtuliang and Hougou gold deposits, North China Craton (Hebei Province, China). Chem Geol 264:101–121

Cook NJ, Halls C, Boyle AP (1993) Deformation and metamorphism of massive sulphides at Sulitjelma, Norway. Mineral Mag 57: 67–81

Cox SF (1987) Flow mechanisms in sulphide minerals. Ore Geol Rev 2:133–171

Cox SF, Etheridge MA, Hobbs BE (1981) The experimental ductile deformation of polycrystalline and single-crystal pyrite. Econ Geol 76:2105–2117

Craig JR (2001) Ore-mineral textures and the tales they tell. Can Mineral 39:937–956

Craig JR, Vokes FM (1992) Ore mineralogy of the Appalachian–Caledonian stratabound sulfide deposits. Ore Geol Rev 7:77–123

Craig JR, Vokes FM (1993) The metamorphism of pyrite and pyritic ores: an overview. Mineral Mag 57:3–18

Craig JR, Vokes FM, Solberg TN (1998) Pyrite: physical and chemical textures. Miner Deposita 34:82–101

Davis GH, Reynolds SH (1996) Structural geology of rocks and regions. Wiley, New York

Etheridge MA, Wall VJ, Vernon RH (1983) The role of the fluid phase during regional metamorphism and deformation. J Metamorph Geol 1:205–226

Freitag K, Boyle AP, Nelson E, Hitzman M, Churchill J, Lopez-Pedrosa M (2004) The use of electron backscatter diffraction and orientation contrast imaging as tools for sulphide textural studies: example from the Greens Creek deposit (Alaska). Miner Deposita 39:103–113

Gaspar O, Pinto A (1991) The ore textures of the neves-Corvo volcanogenic massive sulphides and their implications for ore beneficiation. Mineral Mag 55:417-422

Gee DG, Sturt BA (1985) The Caledonide orogen: Scandinavia and related areas. Wiley, New York

Gill GE (1969) Experimental deformation and annealing of sulphides and interpretation of ore textures. Econ Geol 64:500–508

Graf JL, Skinner BJ (1970) Strength and deformation of pyrite and pyrrhotite. Econ Geol 65:206–215

Graf JL, Skinner BJ, Bras J, Fagot M, Levade C, Couderc JJ (1981) Transmission electron–microscopic observation of plastic-deformation in experimentally deformed pyrite. Econ Geol 76:738–742

Grenne T (1987) Marginal basin type metavolcanites of the Hersjo Formation, eastern Trondheim District, Central Norwegian Caledonides. Nor Geol Unders 412:29–42

Grenne T, Ihlen PM, Vokes FM (1999) Scandinavian Caledonide metallogeny in a plate tectonic setting. Miner Deposita 34:422–471

Hacker BR, Gans PB (2005) Continental collisions and the creation of ultrahigh-pressure terranes: petrology and thermochronology of nappes in the central Scandinavian Caledonides. GSA Bulletin 117:117–134

Henning-Michaeli C (1985) Slip along <-311> and <-3–11> on 112 in experimentally deformed chalcopyrite. Fortschr Mineral 63:93

Ihlen PM, Grenne T, Vokes FM (1997) Metallogenic evolution of the Scandinavian Caledonides. Trans Inst Min Metall 106:194–203

Jansen EM, Siemes H, Brokmeier HG (1998) Crystallographic preferred orientation and microstructure of experimentally deformed Braubach galena ore with emphasis on the relation to diffusional processes. Miner Deposita 34:57–70

Mainprice D (1990) An efficent Fortran program to calculate seismic anisotropy from the lattice preferred orientations of minerals. Comput Geosci 16:385–393

Mann S, Sparks NHC, Frankel RB, Bazylinski DA, Jannasch HW (1990) Biomineralization of ferromagnetic greigite (Fe3S4) and iron pyrite (FeS2) in a magnetotactic bacterium. Nature 343:258–261

Marshall B, Gilligan LB (1987) An introduction to remobilization: information from ore-body geometry and experimental considerations. Ore Geol Rev 2:87–131

Marshall B, Gilligan LB (1993) Remobilization, syntectonic processes and massive sulfide deposits. Ore Geol Rev 8:39–64

Marshall B, Vokes FM, Larocque ACL (2000) Regional metamorphic remobilisation: upgrading and formation of ore deposits. In: Spry, PG, Marshall, B, Vokes, FM (eds) Metamorphosed and metamorphogenic ore deposits. Reviews in economic geology 16: 19–38

McCaffrey K, Lonergan L, Wilkinson JJ (1999) Fractures, fluid flow and mineralization Geological Society of London Special Publication. London 155:328

McClay KR, Ellis PG (1983) Deformation and recrystallization of pyrite. Mineral Mag 47:527–538

McClellan EA (2004) Metamorphic conditions across the Seve-Köli Nappe boundary, southeastern Trondheim region, Norwegian

Caledonides: Comparison of garnet-biotite thermometry and amphibole chemistry. Nor J Geol 84:257–282
McQueen KG (1987) Deformation and remobilization in some Western Australian nickel ores. Ore Geol Rev 2:269–286
Michibayashi K, Mainprice D (2004) The role of pre-existing mechanical anisotropy on shear zone development within oceanic mantle lithosphere: an example from the Oman ophiolite. J Petrol 45:405–414
Mookherjee A (1976) Ores and metamorphism: temporal and genetic relationships. Elsevier, Amsterdam
Mücke A, Younessi R (1994) Magnetite-apatite deposits (Kiruna-type) along the Sanandaj-Sirjan zone and in the Bafq area, Iran, associated with ultramafic and calcalkaline rocks and carbonatites. Mineral Petrol 50:219–244
Nilsen O, Corfu F, Roberts D (2007) Silurian gabbro-diorite-trondhjemite plutons in the Trondheim Nappe Complex, Caledonides, Norway: petrology and U-Pb geochronology. Nor J Geol 87:329–342
Nilsen O, Sundvoll B, Roberts D, Corfu F (2003) U-Pb geochronology and geochemistry of trondhjemites and a norite pluton from the SW Trondheim Region, Central Norwegian Caledonides Norges geologiske undersøkelse. Bulletin 441:5–16
Nilsson LP, Sturt BA, Ramsay DM (1997) Ophiolitic ultramafites in the Folldal-Røros tract and their Cr-(PGE) mineralisation. Nor Geol Unders 433:10–11
Ohfuji H, Boyle AP, Prior DJ, Rickard D (2005) Structure of framboidal pyrite: an electron backscatter diffraction study. Am Mineral 90:1693–1704
Passchier CW, Trouw RAJ (2005) Microtectonics. Springer, Berlin Heidelberg pp 40-51
Prior DJ, Wheeler J, Peruzzo L, Spiess R, Storey C (2002) Some garnet microstructures: an illustration of the potential of orientation maps and misorientation analysis in microstructural studies. J Struct Geol 24:999–1011
Roberts D, Gee DG (1985) An introduction to the structure of the Scandinavian Caledonides. In: Gee DG, Sturt BA (eds) The Caledonide orogen, Scandinavia and related areas. Wiley, London, pp 55–68
Roberts D, Wolff FC (1981) Tectonostratigraphic development of the Trondheim Region Caledonides. J Struct Geol 3:487–494
Rui IJ (1972) Geology of the Røros district south-eastern Trondheim region with a special study of the Kjøliskarvene-Holtsjøen area. Nor Geol Tidsskr 52:1–21
Rui IJ, Bakke I (1975) Stratabound sulphide mineralization in the Kjøli area, Røros district, Norwegian Caledonides. Nor Geol Tidsskr 55:51–75
Siemes H, Zilles D, Cox SF, Merz P, Schafer W, Will G, Schaeben H, Kunze K (1993) Preferred orientation of experimentally deformed pyrite measured by means of neutron-diffraction. Mineral Mag 57:29–43
Skauli H, Boyce AJ, Fallick AE (1992) A sulfur isotopic study of the Bleikvassli Zn–Pb–Cu deposit, Nordland, Northern Norway. Miner Deposita 27:284–292
Spry PG (2000) Sulfidation and oxidation haloes as guides in the exploration for metamorphosed sulfide ores In: Spry PG, Marshall B, Vokes FM (eds) Metamorphosed and metamorphogenic ore deposits. Reviews in Economic Geology11:149-161
Sturt BA, Ramsay DM (2002) Early Ordovician terranne-linkages between oceanic and continental ternes in the central Scandinavian Caledonides. Terra Nova 11:79–85
Sturt BA, Ramsay DM, Bjerkgård T (1997) Revisions of the tectonostratigraphy of the Otta-Røros tract. Norges Geol Undersøk Bull 433:8–9
Sundblad K, Andersen T, Beckholmen M, Nilsen O (2006) Ordovician Escanaba type VMS deposits in the Scandinavian Caledonides. 27th Nordic Geological Winter Meeting: 156.
Vernooij MGC, Brok BD, Kunze K (2006) Development of crystallographic preferred orientations by nucleation and growth of new grains in experimentally deformed quartz single crystals. Tectonophysics 427:35–53
Vokes FM (1968) Regional metamorphism of the Paleozoic geosynclinal sulphide ore deposits of Norway. Transactions of the Institute of Mining and Metallurgy 77:53–59
Vokes FM (1969) A review of metamorphism of sulphide deposits. Earth-Sci Rev 5:99–143
Vokes FM (1976) Caledonian massive sulphide deposits in Scandinavia—a comparative review. In: Wolf KH (ed) Handbook of stratabound and stratiform ore deposits. Elsevier, Amsterdam, pp 318–329
Vokes FM (1988) Latest Proterozoic and Phanerozoic metallogeny in Fennoscandia. In: Zachrisson E (ed) Proceedings of the Seventh Quadrennial IAGOD Symposium. Scheweizerbart, Sweden, pp 41–58
Vokes FM, Grenne T, Ihlen PM (2003) Caledonian stratabound base-metal sulphides in Scandinavia. In: Kelly JG, Andrew CJ, Ashton JH, Boland MB, Earls G, Fusciardi L, Stanley G (eds) Europe's major base metal deposits. Irish Association for Economic Geology, Dublin, pp 101–126
Wheeler J, Prior DJ, Jiang Z, Spiess R, Trimby PW (2001) The petrological significance of misorientations between grains. Contrib Mineral Petrol 141:109–124
Wolff FC (1967) Geology of the Meraker area as a key to the eastern part of the Trondheim region. Nor Geol Unders 254:123–146
Xu G (1996) Structural geology of the Dugald River Zn-Pb-Ag deposit, Mount Isa Inlier, Australia. Ore Geol Rev 11:339–361
Zhang Y, Wilson CJL (1997) Lattice rotation in polycrystalline aggregates and single crystals with one slip system: a numerical and experimental approach. J Struct Geol 6:875–885